We are IntechOpen, the world's leading publisher of Open Access books Built by scientists, for scientists

4,800
Open access books available

122,000
International authors and editors

135M
Downloads

Our authors are among the

154
Countries delivered to

TOP 1%
most cited scientists

12.2%
Contributors from top 500 universities

CLARIVATE ANALYTICS BOOK CITATION INDEX INDEXED

WEB OF SCIENCE™

Selection of our books indexed in the Book Citation Index in Web of Science™ Core Collection (BKCI)

Interested in publishing with us?
Contact book.department@intechopen.com

Numbers displayed above are based on latest data collected.
For more information visit www.intechopen.com

14

Piezoelectric Thick Films: Preparation and Characterization

J. Pérez de la Cruz
INESC Porto - Institute for Systems and Computer Engineering of Porto, Porto, Portugal

1. Introduction

Sol-gel technology allows the deposition of 1μm thick oxide films onto a variety of substrates at temperatures well below those conventionally used for bulk ceramic processing. Thin film processing temperatures as low as 500-700ºC are typically used allowing ceramic materials to be incorporated into the silicon processing stages (Ohno et al., 2000; Wu et al., 1999). In addition, low processing temperatures reduce the inter-diffusion of atomic species between the different thin film layers and ionic vaporization, such as: lead in lead zirconate titanate oxide (PZT) films (Wu et al., 1999; Jeon et al., 2000). PZT thin films have been largely deposited in order to produce several types of devices, such as: membrane sensors, accelerometers and micromotors (Barrow et al., 1997). However, devices requiring larger actuation forces (i.e. high frequency transducers, vibration control devices) require thicker piezoelectric films (Tsurumi et al., 2000). In these cases, it is not practical to produce thick PZT films using standard sol-gel techniques, because of the increased cracking risk due to shrinkage nor is it desirable to produce thick films by a repetitive single layer deposition process due to the time required (Barrow et al., 1995; Zhou et al., 2000).

The interest in ferroelectric lead zirconate titanate thick films for device applications, including high-frequency ferroelectric sonar transducers (Bernstein et al., 1997), micro-electromechanical system devices (Polla & Schiller, 1995; Myers et al., 2003; (Akasheh et al., 2004), elastic surface wave devices (Cicco et al., 1996), hydrophones (Chan et al., 1999) and sensors (Xia et al., 2001), has increased in the last decades because PZT ferroelectric thick films possess the merits of both bulk and thin film materials (Barrow et al., 1997; Ledermann et al., 2003). PZT thick films devices not only work at low voltage and high frequency, as they are compatible with semiconductor integrated circuit, but also possess superior electric properties approaching near-bulk values. Naturally, processing of PZT thick films has also become an increasingly popular research field. Some approaches that have recently been studied to process thick films include electrophoretic deposition (Corni et al., 2008), pulsed laser deposition (Yang et al., 2003), screen printing (Walter et al., 2002) and sol-gel (Xia et al., 2001; Wang et al., 2003; He et al., 2003). Among them, the hybrid sol-gel technique has a special interest due to its low preparation cost and excellent stoichiometric control. Sol-gel also offers the capability to lay down thick layers anywhere between 0.1μm and 100μm, a thickness range that is difficult to achieve by other deposition techniques.

In this chapter an exhaustive review of the preparation of PZT thick films by infiltration method will be presented. Solution powder agglomeration, film densification, phase formation temperature, among others, will be some of the topics that will be analyzed. Finally, the structural and electrical properties of the PZT thick films as a function of the number of solution infiltrations will be highlighted.

2. Formation and structural characterization of the thick PZT films

2.1 Flow diagram of hybrid PZT films

It is well-accepted that hybrid powder sol gel coating technology is an excellent technique to develop high quality thick ceramic films of more than 1μm, while all the benefits of sol gel, i.e. ease of fabrication, ability to coat complex geometries and relative cost effectiveness, remains intact (Barrow et al., 1997; Barrow et al., 1995; Dorey et al., 2002, Pérez et al., 2007). It is also known that high-quality lead zirconate titanate (PZT), yttria- and ceria-stabilized zirconia, titania, silica and alumina thick films with more than 100 μm could be fabricated by this method (Barrow et al., 1995). However, questions remain; for instance, which are the advantages and disadvantages of this method?

It is clear that the advantages of the method are associated with the possibility to obtain high-performance thick films with up to 100μm on a variety of substrate material and shapes, but what about the disadvantages? The main problem of this method is associated with the difficulty to obtain dense films that reproduce the ceramics properties. This problem affects all type of thick films; however, it is more pronounced in ferroelectric materials like PZT, where the dielectric, ferroelectric and piezoelectric properties are highly influenced by the film densification.

The preparation process of thick films, specifically PZT, is divided into two main steps: i) the selection of the sol-gel matrix and ii) the dispersion of the PZT precursor powder in the sol-gel matrix. The sol-gel matrix is selected taking into account its composition, viscosity, and endurance to aging, etc. Once the selection of the sol-gel matrix is completed, the second step is the dispersion of the PZT powder into PZT sol-gel matrix. The powder dispersion process guarantees the homogeneity of the suspension and eliminates the possibility of agglomerate formation.

Several authors have considered that this step is fundamental in the preparation of high quality thick films (Barrow et al., 1997; Barrow et al., 1995; Pérez et al., 2007; Kholkin et al., 2001; Simon et al., 2001], because it determines the powder agglomeration degree and subsequent densification of the films. Few authors have showed that the level of powder agglomeration inside the sol gel matrix depends on the shape and size and the method used to obtain these powders (Simon et al., 2001). Moreover, it is consensual that agglomeration increases with time, due to the surface tension force and the sedimentation process.

To avoid the agglomeration process that take places before and during the thick film preparation, some authors have used organic dispersants (i.e., buthoxyethoxy-ethyl acetate (BEEA)), high molecular weight solvents (i.e., α-terpineol), binders (i.e., polyvinyl butyral (PVB)) and plasticizers (i.e., polyethylene glycol (PEG)). Figure 1 shows the grain size distribution of PZT and PT powders prepared by different synthesis routes, which were dispersed using the above-mentioned compounds (Simon et al., 2001). It is clear that powder preparation processes and consequently grain size and shape have a fundamental role in the powder agglomerate formation. For instances, PZT powder prepared by conventional solid

state oxide methods (dry method or DM) shows a mean grain size of 2.2 μm, while PZT powder prepared by a coprecipitation process (web method or WM) shows a mean grain size of 1.9 μm. Some readers could assume that a progressive decrease in powder size could contribute to a smaller powder agglomeration inside the sol-gel matrix, improving the films densification. However, this is not completely true, as when the power size decreases, the effective surface of the powder increases. This increase in the powder effective surface results in an increase of the surface tension force, which strongly contribute to agglomerate formation. An evident example can be observed in Fig. 1, the coprecipitation process produces smaller grain size PZT powders; however, during the sol-gel PZT power mixture a ~10 μm agglomerated is observed.

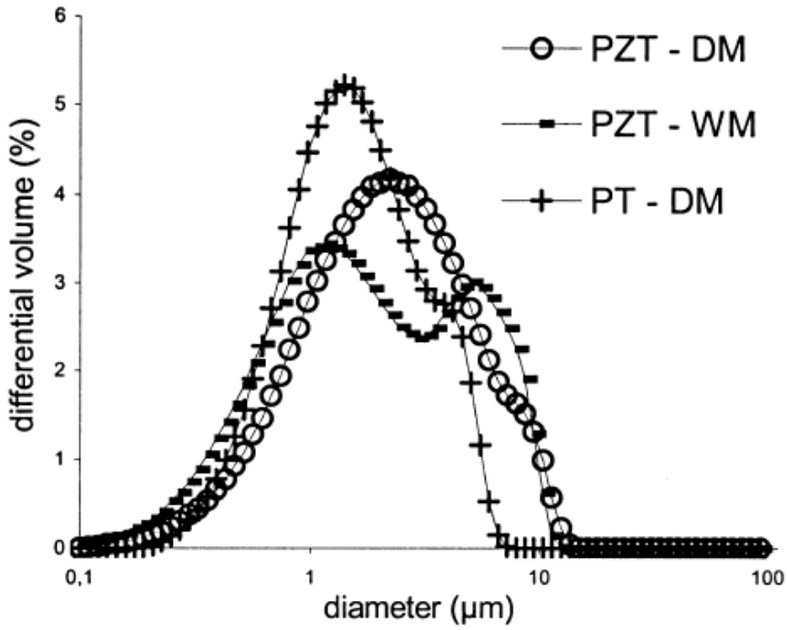

Fig. 1. Grain size distribution of PZT and PT powders prepared by different synthesis routes, and dispersed using α-terpineol solvent, BEEA dispersant, PVB binder and PEG plasticizer (Simon et al., 2001). (Copyright Elsevier)

Similar agglomeration behavior is also observed in high molecular weight free sol gel matrixes. In this case authors have used an ultrasonic dispersion process combined with a relatively high viscous sol-gel matrix in order to eliminate the PZT powder agglomeration (Pérez et al., 2007). As the ultrasonic dispersion time increases, agglomerate formation decreases, as shown in Fig.2. It is clear that the ultrasonic process disperses the agglomerates resulting in an increase of low diameter differential volume. The reduction of the PZT powder agglomeration and the increase in the low diameter differential volume improve the densification of the film during the preparation and reduce the formation of *closed pores*, which cannot be filled by any post-deposition process, such as: infiltration.

It is notable that the ultrasonic process eliminates the agglomerate formation; moreover, it also negates the use of the high molecular weight solvents, dispersants, binders and plasticizer, resulting in shorter drying and pre-annealing processes during the thick film preparation process. The elimination of high molecular weight compounds from the sol-gel matrix reduces in large scale pore formation, improving the PZT thick films densification.

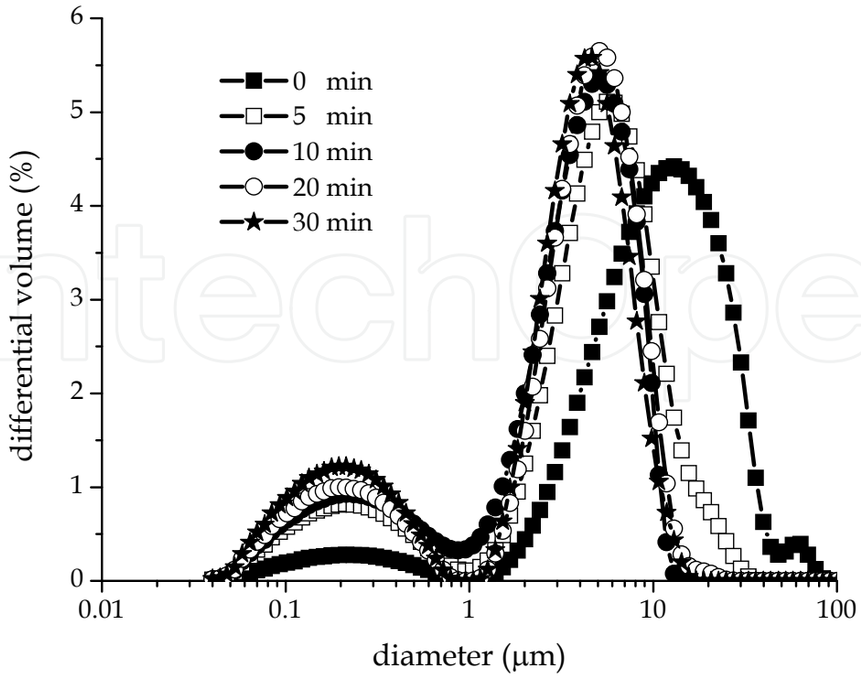

Fig. 2. Distributions of the TRS600 PZT powder particle under different ultrasonic mixing times (Pérez et al., 2007). (Copyright Elsevier)

Hybrid sol-gel/powder formation is followed by the film preparation process. The PZT thick film preparation process practically does not differ to the standard sol-gel thin film preparation (Barrow et al., 1997; Barrow et al., 1995; He et al., 2003; Dorey et al., 2002; Pérez et al., 2007; Kholkin et al., 2001). It is known that PZT thick films could be deposited in several types of substrates; however, it is common that PZT thick films are deposited onto platinized silicon wafers ($Pt/Ti/SiO_2/Si$), due to the higher conductivity of the platinum (Barrow et al., 1995). Prior to the coating step the substrate should be cleaned to remove the substrate dirt. It is usual that the removing of any residual organics of the substrate surface involves low molecular weight volatile compounds, such us: methanol, ethanol, isopropanol, and acetone, among others. However, other techniques like ultrasonic bath and plasma etching are regularly used during the substrate cleaning process (Dorey et al., 2002; Pérez et al., 2007). Afterward, PZT thick films are grown up by depositing a consecutive number of layers. Each layer consists of an initial composite layer, which is deposited by covering the entire wafer surface with the composite slurry and then spinning for 30 s to 60 s in the 2000-4000 rpm spinning frequency range. The spinning frequency and time are normally optimized in order to obtain the desire thickness of each individual layer, which depends on the powder mean size and also on the viscosity of the sol-gel matrix.

Each individual layer is then subjected to a heat treatment process at an intermediate temperature designed to remove the organic component and to pyrolise the PZT sol-gel. This heat treatment process is divided in two step: 1) the drying process, which is carried out from 100ºC up to 300ºC during ~60 s and 2) the pre-annealing process (or calcination) that is carried in the 300ºC-500ºC temperature range form few seconds up to various minutes (Barrow et al., 1997; Barrow et al., 1995; He et al., 2003; Dorey et al., 2002; Pérez et al., 2007; Kholkin et al., 2001). The drying and pre-annealing temperature used in the heat

treatment of each layer should take into account the type of solvent and the organic compounds utilized in the preparation of the PZT sol-gel matrix and also the stoichiometry of the material that is to be prepared. For that reason, prior to the preparation process it is convenient to carry out the decomposition analysis of the sol-gel matrix by using thermogravimetric and differential thermal analysis techniques. These techniques supply the characteristic decomposition temperatures of the sol-gel matrix. Drying and/or pre-annealing the PZT *green* layers above the characteristic temperatures should be carried out gradually, because it could result in the formation of cracks.

On the other hand, PZT thick films prepared by a sol gel matrix rich in high molecular weight compounds, like dispersants, binders and plasticizers, show long drying and pre-annealing processes that range from 1 hour up to 24 hours. The long time drying and pre-annealing processes are necessary in order to evaporate the solvents and burn all the high molecular weight organic compounds used in the PZT sol-gel matrix preparation avoiding, therefore, the formation of crack in the films.

Once the desire thickness is obtained the whole film is subjected to a crystallization stage where the pre-annealing sample is sintered at higher temperatures designed to develop the perosvkite phase. In the case of PZT thick films the sintering temperature (also known as annealing temperature) can vary from 400ºC up to 800ºC as a function of the zirconium/titanium ratio, while the annealing time could go from 30 up to 60 minutes. Using this technique, several authors have prepared thick, crack free PZT films (Barrow et al., 1995; Dorey et al., 2002; Pérez et al., 2007). However, Barrow *et. al.,* (Barrow et al., 1995) were the first to attribute the crack free nature of these films to i) the presence of large amounts of powder that results in a decrease of the level of sol-gel present and hence lower shrinkage; (ii) strong bonding between the sol-gel and the PZT particles making cracking less likely.

On the other hand, Wu *et. al.,* (Wu et al., 1999) proved that the incorporation of PZT powder into the PZT sol-gel solution shows additional benefits. The addition of ~1 wt.% of PZT powder decreases the perovskite formation temperature by 50 ºC, increasing substantially the dielectric and ferroelectric properties of these films (Wu et al.,1999). It is believed that the incorporation of PZT micro-powders in a PZT sol-gel matrix promotes heterogeneous nucleation of the perovskite phase coming from the sol-gel, resulting in a randomly orientated PZT film.

Dorey *et. al.*, (Dorey et al., 2002) and Pérez *et. al.*, (Pérez, 2004) observed that a graded structure is obtained when the PZT thick film is not infiltrated with the precursor PZT sol-gel solution, during the preparation process. This graded structure results because the sol-gel is drawn from the slurry into the underlying porous composite layer (Dorey et al., 2002). It is believed that as the number of layers increased, the lower composite layers become further enriched with sol-gel. Thus, the bottom composite layer of a four layer structure will be effectively infiltrated three times (Dorey et al., 2002). It is evident that the infiltration of the bottom layer is conditioned by the porous infiltration saturation. Pérez *et. al.*, observed that there is a progressive infiltration of PZT graded structure up to four infiltrations (Pérez, 2004). However, at higher infiltrations the porosity of the bottom layer practically does not change, which can be further explained based on Darcy´s law (Scheidegger, 1974).

It is consensual that the formation of a graded structure is detrimental to the dielectric, ferroelectric and piezoelectric properties of the PZT thick films. Hence, an intermediate

infiltration of each individual composite layer and a final infiltration of the whole film are necessary, leading to a homogenization of the film structure, fixing the graded structural problem, as shown by Perez and co-workers (Pérez et al., 2007; Pérez, 2004). The infiltration of each individual layer with sol-gel prior to the deposition of the next composite layer results in a relative densification of the layer and a strengthening of the powder compact without shrinkage, while the final infiltration is used to improve the PZT thick film surface (Tu et al., 1995). Thus, with this method it is possible to produce high-quality PZT thick composite films with uniform densities and good surfaces.

2.2 Infiltration of the PZT thick films

It was mentioned above that the infiltration process of the PZT thick film could be explained based on Darcy´s law (Scheidegger, 1974). The experiments of Darcy were focused on the volumetric flow rate (Q) of the fluid through a sand column, which is similar to the infiltration of a sol-gel solution through a porous film. It can be observed that flow occurs only in the pore space. Thus, the effective area of flow is not the entire column cross section (A), but this area multiplied by the porosity (μ·A). Note that although the porosity μ is a volume fraction, it is also useful in determining an average effective area of flow. Thus the average speed of the macroscopically one-dimensional flow in a cross section of Darcy's column relative to the solid grains is:

$$\left| v^l - v^s \right| = \frac{Q}{\mu A} \tag{1}$$

where v^l is the velocity of the liquid in a porous media and v^s is the velocity of the media. It is clear that in the thick films case the velocity of the media is ~0.

Taking into account that Darcy demonstrated experimentally that the volumetric flow rate of a liquid (i.e., water) down through the porous medium is proportional to the head difference across the sand column ($h_2 - h_1$), and the cross sectional flow area and is inversely proportional to the packed height of the column (L), such that:

$$Q = KA\left|\frac{h_2 - h_1}{L}\right| \tag{2}$$

where K is referred to as hydraulic conductivity (or permeability of the porous body) and it is a function of both the porous medium and the fluid properties, being practically constant for a particular packing even when the flow rate in the column changes. One can obtain the differential form of Darcy´s law, combining the equations 1 and 2 when the limit of the column length is reduce (L→0), as shown:

$$\mu(v^l - v^s) = K^l \frac{dh}{dz} \tag{3}$$

where the hydraulic conductivity (K^l) has been labelled with a superscript (l) to emphasize that in a particular medium, its value will depend on the properties of the fluid phase.

$q^l = \varepsilon(v^l - v^s)$ In a general case the Darcy velocity can be represented in terms of the gradient of pressure elevation heads as:

$$q^l = \frac{K^l}{\rho g}(\nabla P - \rho g) \tag{4}$$

where ρ is the density of the liquid and P the pressure experimented by the liquid. This equation is accurate when the pressure gradient in the liquid column is balanced by gravitational forces. For this equilibrium state, the Darcy velocity is zero. The equations propose that for a "small" imbalance in the gradients that drive the flow, the Darcy expressions reasonably describe the velocity (or infiltration velocity). Confirming experimental evidence indicates that Darcy's correlation is a useful expression to describe flow through porous medium (Scheidegger, 1974). It is clear that the Darcy velocity is not a true velocity of the fluid but represents an effective flow rate through the porous medium.

Several pressures could influence the infiltration process. However, it can be resumed to three main pressures, the applied pressure *Pa* (which includes the hydrostatic pressure), the capillarity force *Pc* and the internal opposing pressure of the compressed gas *Pi*, as shown by Kholkin et. al., (Kholkin et al., 2001). During a "static" infiltration, such as used during a dip-coating process, the infiltration is mainly dominated by the hydrostatic pressure, the capillarity pressure and the internal opposing pressure of the compressed gas; however, during a "dynamic" infiltration, such as used during a spin-coating process, the infiltration is mainly dominated by the applied pressure due to the centrifugation process.

Kholkin et al., (Kholkin et al., 2001) has predicted based on the modified Darcy´s law reported by Scheidegger et. al., (Scheidegger, 1974) (see Equation 5) that for a static infiltration process, where the flow of the liquid into the porous media in controlled by the capillarity pressure, the distance of liquid introduced in the PZT thick film (z) during the time (t=30s) is ≈ 2mm.

$$z = \left(\frac{2KP}{\eta}\right)^{\frac{1}{2}} t^{\frac{1}{2}} \tag{5}$$

This value is 200 times greater than the thickness of the PZT thick film deposited in this study (~10nm). Authors suggest that this value was reached because they did not take into account the increase of the internal opposing pressure of the compressed gas due to the no evacuation of the replaced gas (Kholkin et al., 2001). However, there are other factors like the viscosity of the solution and the permeability of the porous body that should be taken into account. It is known that as the number of infiltrations increase, the viscosity of the solution increases, resulting in a decrease of the infiltration depth (Dorey et al., 2002). On the other hand, the permeability of a powder compact is expressed by the Kozeny-Carman expression:

$$K = \frac{D^2(1-\rho)^3}{36C\rho^2} \tag{6}$$

where D is the average grain size and C de is a parameter that define the shape and tortuosity of the porous channel (Scheidegger, 1974). The C value for a powder compact is estimated as ≈5; however, it increases exponentially as the number of infiltrations increase, mainly because the porous size is reduced. It is believed that this is the major factor that reduces the infiltration depth in powder compact in general and in PZT thick films in particular.

In the next section, one analyzes the effect of the number of top infiltrations in structural, dielectric and piezoelectric properties of a intermediate infiltrated PZT thick film. Moreover, the dielectric properties of the infiltrated PZT thick films will be simulated based on 0-3 and cube ceramic/ceramic composite models, where the numbers 0 and 3 describe the connectivity of the two phases of the material (i.e., the sol gel matrix interconnected in the three directions (3) whereas PZT powder particles are not connected in any direction (0)) (Newnham et al., 1978). Finally, the structural and electrical results will be compared with the ones reported by Dorey *et. al.,* and Ohno *et al.,* in PZT thick film infiltrated with a high molecular weight prepared PZT solution (Ohno et al., 2000; Pérez et al., 2007).

3. Structural, electric and piezoelectric characterization of the PZT thick films

3.1 Structural and microstructural characterization of the infiltrate PZT thick films

There are practically no differences between the structural and microstructural characterizations of thin and thick PZT films. However, it should be taken into account that PZT thick film phase formation, grain growth, crack formation, etc., are highly conditioned by the precursor powder and the powder agglomerate formation, while in PZT thin films they are mainly conditioned by the substrate structure, the characteristic of the PZT precursor solution and the preparation conditions.

3.1.1 Structural characterization of the precursor powder and the infiltrated PZT thick films (X-ray analysis)

Prior to the structural characterization of the PZT thick films it is important to carry out the precursor powder characterization. Figure 3 a) shows the X-ray diffraction pattern of the PZT TRS600 precursor powder used in the preparation of infiltrated PZT thick films (Pérez et al., 2007, Pérez, 2004). The diffraction pattern of this PZT powder shows the presence of a pure perovskite PZT phase and two marginal extra diffraction peaks (26.8º and 33.12º) that are associated with the lead excess and other additives (such as Nb_2O_5) used in the preparation of the commercial PZT powders (TRS, 1998, Kholkin et al., 2000). Normally, the additive compounds used in the preparation of commercial PZT powder have the objective of improving its dielectric and piezoelectric properties. However, they also show extra attributes when the PZT powders are used in the preparation of PZT thick films. For instances, the lead oxide excess present in the PZT precursor powder guarantee that the PZT thick films remain stoichiometric after the annealing process.

Figure 3b) shows the X-ray diffraction patterns of PZT thick films prepared with different number of top infiltrations. The analysis of the (110) PZT diffraction peak shows a decrease of the width and a small shift of the peak position, relatively to the TRS600 PZT commercial powder, as the number of infiltration steps increases. It is evident that the infiltration process reduces the PZT thick film surface roughness, which results in a better relation between incident and diffraction angle of the films. For that reason, the decrease in the width of the (110) PZT diffraction peak is mainly attributed to the decrease of the surface roughness.

In contrast, the shift in the peak position of the maximum as the number of top infiltration layers increase, has been associated with two factors: i) a small difference between PZT powder and PZT solution compositions and ii) a change in the stress of the films provoked by the infiltration cycle, which somehow compacts the film structure.

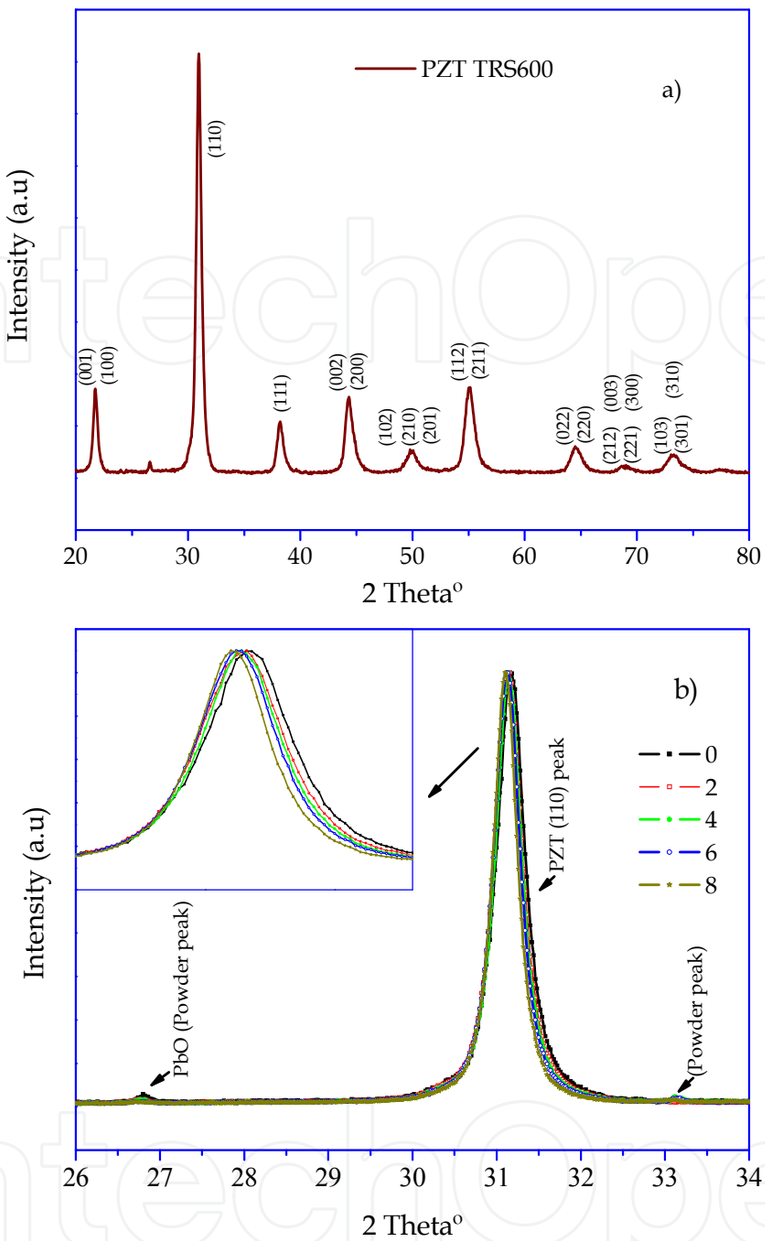

Fig. 3. X-ray diffraction patterns of a) TRS600 PZT precursor powder and b) PZT thick films prepared with different number of top infiltrations (0, 2, 4, 6, and 8) (Pérez et al., 2007). (Copyright Elsevier)

Finally, a decrease in the intensity of the extra TRS600 X-ray diffraction peaks (visible at 26.8° and 33.12°) is observed, showing that as the number of infiltrations increase the factional volume of the formed sol-gel PZT phase is more palpable. This fact emphasizes the idea that as the number of infiltrations increases the number of pores decreases due to a complete coverage by the sol-gel solution. Moreover, the decrease in the 26.8° X-ray diffraction peak could be also associated with the possible evaporation of the lead oxide during the PZT thick film heat treatment process.

3.1.2 Microstructural characterization of the infiltrated PZT thick films (SEM analysis)

Following the crystallographic structural analysis, the microstructural analysis of standard and infiltrated PZT thick films reveals important aspects like: surface roughness, surface cracks, powder agglomeration, film thickness, porosity, among others. When the film is not infiltrated it is easy to observe cracks and small powder agglomerates in the surface of the films, while after few infiltrations the PZT thick films show a smoother and crack-free surface, as shown in Fig.4. It is visible that the infiltration process results in a decrease of the film porosity, increasing the connectivity of the composite films. This fact is extremely important in order to improve the dielectric and ferroelectric properties of the PZT thick films. Moreover, the infiltration process also reduces the film surface roughness, which is helpful for a good adhesion between the film and the top electrode and for a correct estimation of the thickness of the films that will be used in the further calculation of the dielectric and ferroelectric properties.

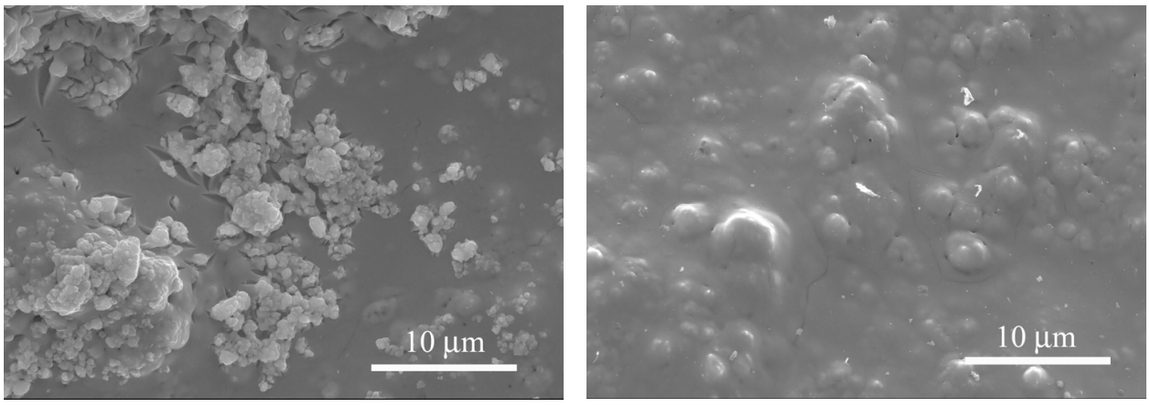

Fig. 4. SEM plan-view images of the PZT thick films with 0 (left) and 8 (right) top infiltrations (Pérez et al., 2007). (Copyright Elsevier)

Figure 5 shows the SEM cross-section microstructure images of the PZT thick films prepared with 0 and 8 top infiltrations. Relatively dense microstructure is observed in the film with 8

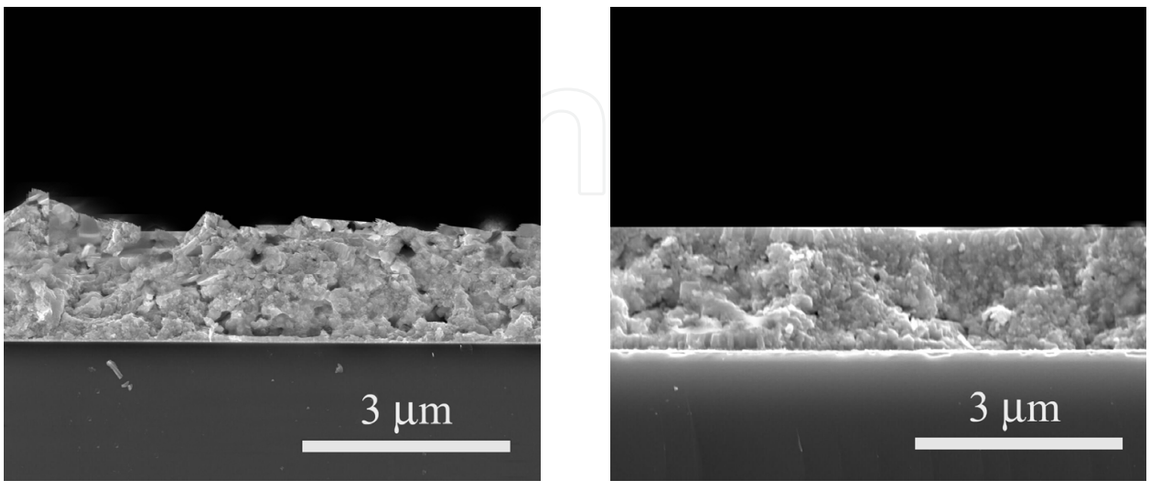

Fig. 5. SEM cross section images of the PZT thick films after 0 (left) and 8 (right) top infiltrations (Pérez et al., 2007). (Copyright Elsevier)

infiltrations, while film without infiltration shows a porous structure mainly in the last deposited layer. It is also visible in the cross section images that the infiltration process results in a decrease of the film porosity; however, there is some remaining porosity that cannot be eliminated. It is called *internal or closed porosity* and results from a premature closing up of the pores channels.

Dorey et al., report a similar behavior in infiltrated PZT thick films using a high molecular weight precursor solution, as shown in Fig. 6 (Dorey et al., 2002). We can see that in films with four infiltrations of this solution, the internal porosity is higher than those reported by Pérez et. al., (Pérez, 2004). It is believed that the higher closed porosity observed in these films result from the increase of the density and viscosity of the precursor solution. Nevertheless, other factors like average grain size and shape and tortuosity of the pore channel should be also taken into account.

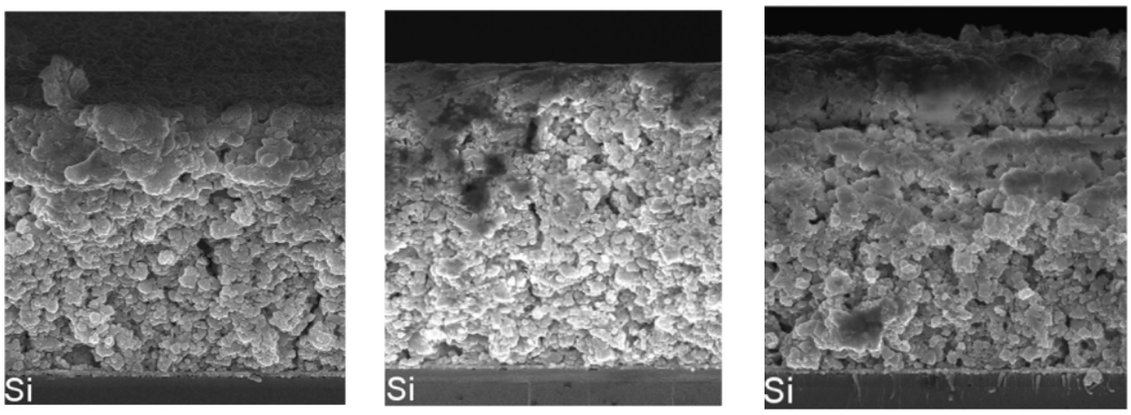

Fig. 6. SEM cross section images of the PZT thick films after 0 (left), 2 center and 4 (right) infiltrations using a high molecular weight precursor solution (Dorey et al., 2002). (Copyright Elsevier)

Surface roughness and porosity can be responsible for the possible deterioration of the dielectric constant and polarization values and the increase dielectric losses in PZT thick film. As mentioned, they are highly affected by the infiltration process. For this reason, in the next section one presents the dielectric, ferroelectric and piezoelectric behavior of the PZT thick films as a function of the number of infiltrations.

4. Electrical properties of the PZT thick films as a function of the number of infiltrations

We have already seen that in PZT thick films the structural and microstructural properties are highly dependent on the number of infiltrations, but what about the dielectric, ferroelectric and piezoelectric properties? It is well-known that in bulk materials the dielectric, ferroelectric and piezoelectric properties are highly dependent on grain size, porosity, phase formation, stoichiometric, crystallographic orientation, amongst others. However, in PZT thick films this dependence may be notably different because the electrical properties are also affected by substrate clamping, surface powder agglomeration and the mixture of phases coming from the precursors PZT powder and PZT sol-gel solution, etc.

4.1 Dielectric behavior of the PZT thick films as a function of the number of infiltrations

Figure 7 shows the dielectric constant and dielectric losses behavior reported by Pérez and co-workers for infiltrated PZT thick films (Pérez et al., 2007). It is observable that the dielectric constant increases as the number of infiltrations increase, while the dielectric loss remains around 0.05. This dielectric constant behavior is consistent with the decrease in porosity as the film is infiltrated, reaching its maximum around 2320. This value is far from the 3420 reported on the TRS600 PZT powder (Kholkin et al., 2001, TRS, 1998). However, it should be taken into account that a phase mixture is presented in the PZT thick film, being the dielectric constant of the PZT layer obtained from the sol-gel solution ~1900 (Pérez et al., 2004), and, furthermore, that there is some closed porosity .

The increases in the dielectric constant as the number of infiltrations increase could be easily explained based on connectivity models (Barrow et al., 1997; Kholkin et al., 2001). These models describe the connectivity degree between the PZT powders particles inside the PZT films matrix formed after the deposition process.

4.1.1 Dielectric constant models for connected composite material

Based on the deposition process of the PZT infiltrated thick films reported by Pérez and co-workers, which includes intermediate infiltrations, the dielectric constant might be modeled as a 0-3 composite material, where the sol gel matrix is fully connected in three directions and the ceramic particles (powder) are not connected in any direction. Assuming that the particles are uniformly dispersed in the sol gel matrix, then the resulting dielectric constant can be given by (Moulson & Herbert, 2004):

$$\varepsilon_m = \varepsilon_2 \left[1 + \frac{3 * V_1(\varepsilon_1 - \varepsilon_2)}{\varepsilon_1 + 2 * \varepsilon_2 - V_1(\varepsilon_1 - \varepsilon_2)} \right] \tag{7}$$

where ε_1 is the dielectric constant of the PZT powder, ε_2 is the dielectric constant of the sol gel matrix, and V_1 is the volume fraction of the ceramic powder.

Practically, this equation is only valid for low powder volume fraction values $V_1<0.1$ (Barrow et al., 1997), because at higher concentrations, the dispersed phase starts to form continuous structures throughout the bulk that have nonzero connectivity. However, due to the intermediate infiltration process carried out in the preparation of the PZT thick films the 0-3 connectivity is practically maintained. Thus, this model can be applied for relatively higher powder volume fraction values.

Although the 0-3 connectivity model is not faraway from reality, a more likely scenario is that proposed by Pauer (Barrow et al., 1997; Pauer, 1973], where the material exists in a combination of series and parallel phases (cube model). In this case the effective dielectric constant can be calculated by:

$$\varepsilon_m = \frac{\varepsilon_1 \varepsilon_2}{(\varepsilon_2 - \varepsilon_1) V_1^{-1/3} + \varepsilon_1 V_1^{-2/3}} + \varepsilon_2 (1 - V_1^{2/3}) \tag{8}$$

Assuming that in a highly infiltrated PZT films the powder/solution volume fraction is 0.66/0.33, the dielectric value calculated by both models is ~2580, a little higher than the one obtained in the experimental results (see Figure 8). Note both models did not take into consideration the porosity of the films. For that reason, we could expect lower effective dielectric values than 2580.

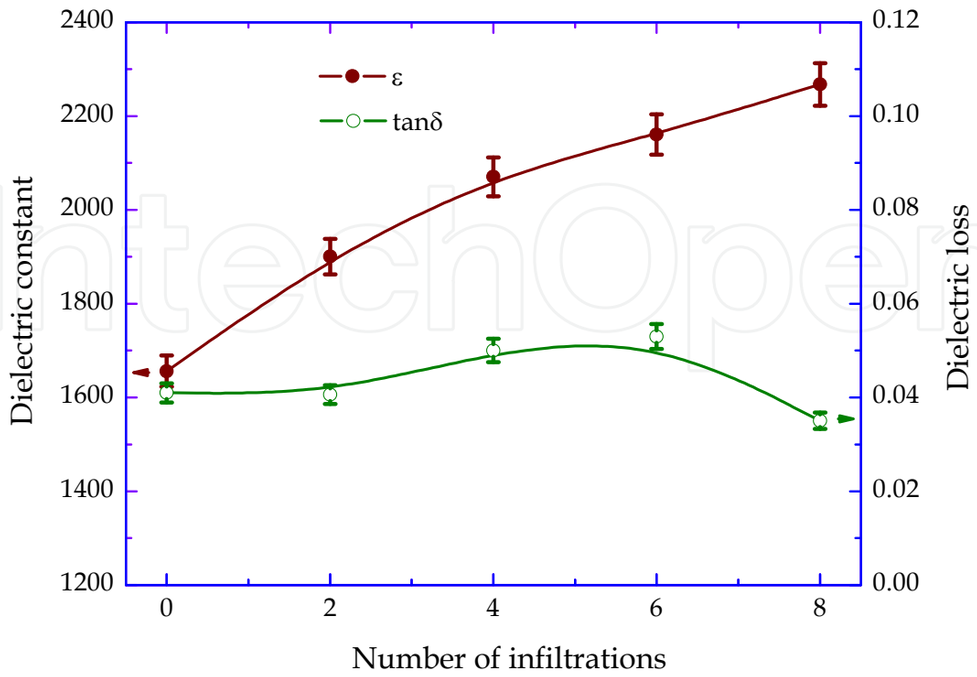

Fig. 7. Dielectric behavior of the PZT thick films, prepared based on a low molecular weight precursor solution, as a function of the number of infiltrations (Pérez et al., 2007). (Copyright Elsevier)

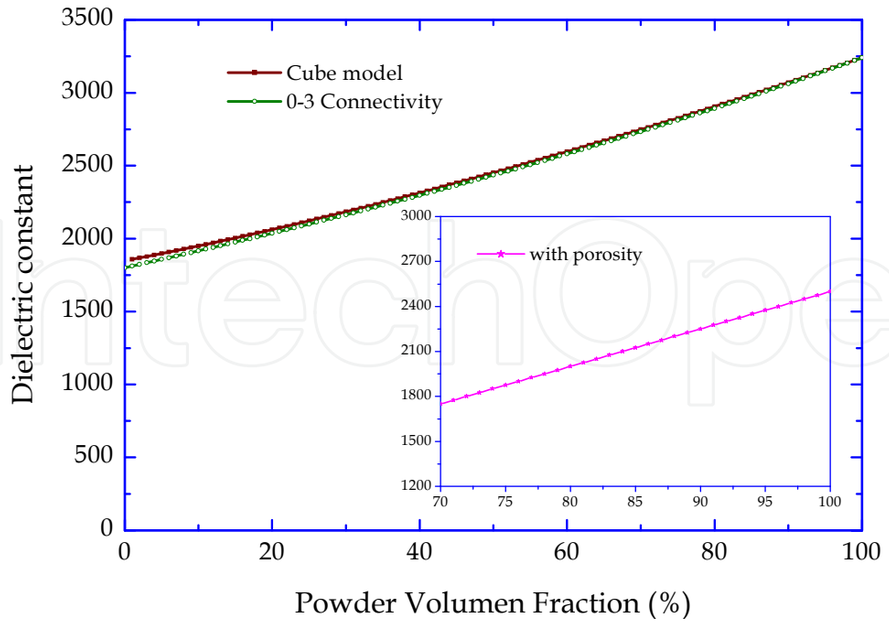

Fig. 8. Dielectric constant of PZT composite predicted by 0-3 composite and cube models. Inset plot shows the dielectric constant values calculated taking into account a 30% to 0% variable porosity in parallel with the PZT composite (0.66/0.33 powder/solution ratio).

In the hypothetic scenario that 8% of the films is free space or porosity filled by air and also that they are connected in parallel with the composite material (powder/solution), the dielectric constant values match with the experimental results (see inset plot Figure 8). At the extremes, one observes deviations from the experimental values due to the irremovable porosity at higher dielectric volume fraction and the actuation of a serial porosity component at a "lower" composite volume fraction. The irremovable porosity is enclosed in the powder agglomeration, which hinder its elimination while the serial porosity contribution appears when the composite films are not infiltrated. It is clear that in non-infiltrated PZT thick films the porosity contributes to both serial and parallel capacitances of the system, degrading the dielectric constant of these films.

4.2 Ferroelectric behavior of the PZT thick films as a function of the number of infiltrations

Figure 9 shows the hysteresis loop of PZT thick films prepared using different number of infiltrations. It is visible that the remnant polarization values increases with the increase of the number of infiltrations. A large remnant polarization in the orders of Pr=35 μC/cm² and a small coercive field Ec=59 kV/cm are obtained in PZT thick film prepared with 8 top infiltrations, as shown in the inset of Figure 9. The remnant polarization value is similar to the one reported for 1μm coating PZT films prepared using a modified solution (Pérez et al., 2004). However, the coercive field is lower suggesting that it is easier to switch the polarization in infiltrated PZT thick films. In this study, the polarization trend results for a decrease of the porosity and improvement of the films surface as the number of infiltration

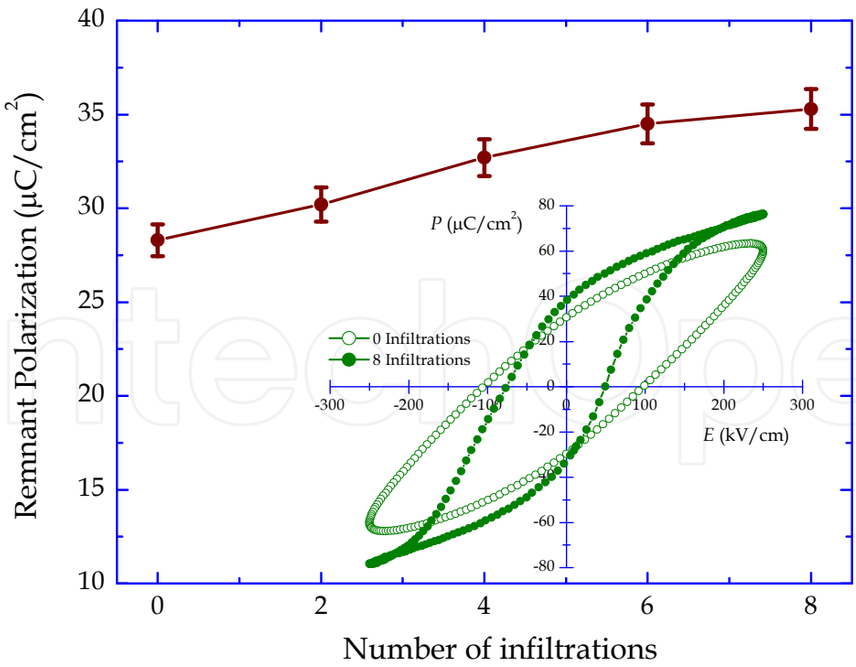

Fig. 9. Remnant polarization of the PZT thick films as a function of the number of top infiltration. Inset plot show the hysteresis loop of the films with 0 and 8 infiltrations (Pérez et al., 2007).

increase. It is comprehensible that as the channel of the pore and the pore size itself are reduced; the infiltration becomes more and more difficult, resulting in a blocking of the infiltration process. The saturation in dielectric constant and remnant polarization also indicates that infiltration and pore size reduction is almost stopped for higher number of infiltrations.

4.3 Piezoelectric behavior of the PZT thick films as a function of the number of infiltrations

Figure 10 illustrates the piezoelectric coefficient as a function of the number of infiltration and the piezoelectric loop of the PZT thick film prepared with 8 top infiltrations. The trend in the piezoelectric coefficient is similar to those reported for the polarization, showing a piezoelectric coefficient (d_{33}) of ~65 pm/V in the films with 8 top infiltrations. It is notable that the piezoelectric coefficients observed in the 8 times infiltrated PZT thick film is of the same order of magnitude as those reported for a 1μm PZT coating films prepared using a modified solution (Pérez et al., 2004). On the other hand, in the non-infiltrated film the piezoelectric coefficient is not reported due to the high surface roughness, which does not allow the piezoelectric measurement of this film.

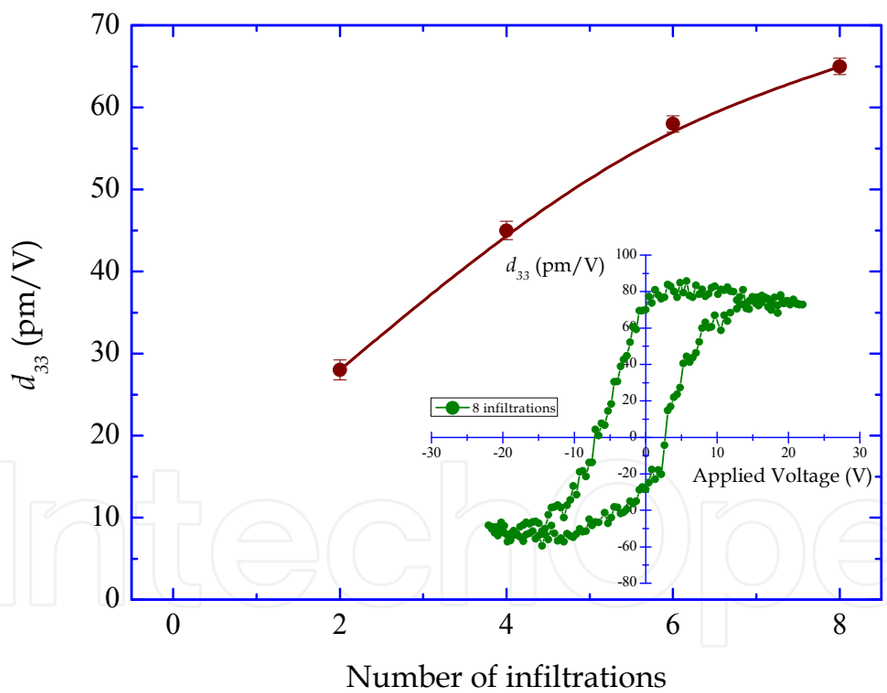

Fig. 10. d_{33} piezoelectric thick film behavior as a function of the number of infiltrations. Inset plot show the piezoelectric loop of the PZT thick films prepared using 8 top infiltrations.

Dorey *et. al.*, reported the same piezoelectric coefficient (~65 pm/V) for PZT thick film infiltrated with a high molecular weight solution (Dorey et al., 2002). The d_{33} coefficients obtained by Dorey and Pérez suggests that the piezoelectric response of the infiltrated PZT thick films is highly conditioned by the piezoelectric response of the PZT phase formed from the sol-gel solution (Dorey et al., 2002; Pérez et al., 2007).

Finally, it should be noted that although the piezoelectric coefficient of highly infiltrated PZT thick film does not reach the piezoelectric coefficient of the PZT ceramics, it is good enough for micromechanical applications. Note it is much higher than for non-ferroelectric piezoelectrics clamping by rigid substrate (ZnO, AlN) (Trolier-McKinstry & Muralt, 1973) and in the same order as that of PZT thin film deposited onto a platinized substrate (Pérez et al., 2004).

5. Conclusion

In this work an exhaustive review on the preparation of PZT thick films have been carried out, taking specific focus in the effect of the infiltration in the preparation of high-quality films. Solution powder agglomeration, films densification, phase formation temperature, among others, have been analyzed. Moreover, the infiltration process is discussed based on Darcy´s law, while the improvement of structural and microstructural properties has been analyzed as a function of the infiltration process. The dielectric properties are characterized as function of the number of infiltrations and the results compared with those obtained by the 0-3 composite connectivity and the cube models. Finally, ferroelectric and piezoelectric properties are also discussed, as function of the number of infiltrations.

6. References

Akasheh, F.; Myers, T.; Fraser, J.; Bose, S. & Bandyopadhyay, A. (2004). Development of Piezoelectric Micromachined Ultrasonic Transducers, *Sensors and Actuators A-Physical*, Vol.111, No.2-3, pp. 275–287

Barrow, D. A., Petroff, T. E. and Sayer M. (1995). Thick Ceramic Coating Using a Sol Gel Based Ceramic-Ceramic 0-3 Composite, *Surface and Coating Technology*, Vol. 76-77, No. 2-3, pp. 113–118

Barrow, D. A.; Petroff, T. E.; Tandon, R. P. & Sayer M. (1997). Characterization of Thick Lead Zirconate Titanate Films Fabricated Using a New Sol-Gel Based Process, *Journal of Applied Phys*ics, Vol.81, No.2, pp. 876–881

Bernstein J. J., Finberg S. L., Houston K., Niles L. C., Chen H. D., Cross L. E., Li K. K., and Udayakumar K. (1997). Micromachined High Frequency Ferroelectric Sonar Transducers, *IEEE Transactions on Ultrasonics Ferroelectric and Frequency Control*, Vol. 44, No.5, pp. 960–969

Chan, H. L. W.; Lau, S. T. & Kwok, K. W. (1999). Nanocomposite Ultrasonic Hydrophones, *Sensors and Actuators A-Physical*, Vol.75, No.3, pp.252–256

Cicco, G. D.; Morten, B. & Prudenziati, M. (1996). Elastic Surface Wave Devices Based on Piezoelectric Thick-Films, *IEEE Transactions on Ultrasonics Ferroelectric and Frequency Control*, Vol.43, No.1, pp. 73–77

Corni, I.; Ryan, M. P. & Boccaccini, A. R. (2008). Electrophoretic Deposition: From Traditional Ceramics to Nanotechnology, *Journal of the European Ceramic Society*, Vol.28, No.7, pp. 1353–1367

Dorey, R. A.; Stringfellow, S. B. & Whatmore, R. W. (2002). Effect of Sintering Aid and Repeated Sot Infiltrations on the Dielectric and Piezoelectric Properties of a PZT Composite Thick Film, *Journal of the European Ceramic Soc*iety, Vol.22, No.16, pp.2921–2926

He, X. Y.; Ding, A. L.; Zheng, X. S.; Qiu, P. S.; & Luo, W. G. (2003). Preparation of PZT(53/47) Thick Films Deposited by a Dip-Coating Process, *Microelectronic Engineering*, Vol.66, No.1-4, pp.865–871

Jeon Y., Chung J., and No K. (2000). Fabrication of PZT Thick Films on Silicon Substrates for Piezoelectric Actuator, *Journal of Electroceramics*, Vol.4, No.1, pp. 195–199

Kholkin, A. L.; Yarmarkin, V. K.; Wu, A.; Vilarinho P. M. & Baptista J. L. (2000). Thick Piezoelectric Coatings via Modified Sol-Gel Technique, *Integrated. Ferroelectrics*, Vol.30, No.1-4, pp.245–252

Kholkin, A.L.; Yarmarkin V.K.; Wu, A.; Avdeev, M.; Vilarinho, P. M. & Baptista, J. L. (2001). PZT-Based Piezoelectric Composites via a Modified Sol-Gel Route, *Journal of the European Ceramic Soc*iety, Vol.21, No.10-11, pp.1535–1538

Ledermann, N.; Muralt, P.; Baborowski, J.; Gentil, S.; Mukati, K.; Cantoni, M.; Seifert, A. & Setter, N. (2003). {100}-Textured, Piezoelectric $Pb(Zr_xTi_{1-x})O_3$ Thin Films for MEMS: Integration, Deposition and Properties, *Sensors and Actuators A-Physical*, Vol.105, No.2, pp. 162–170

Moulson, A. J. & Herbert, J. M. (1990). *Electroceramics*, University Press, Cambridge, UK

Myers, T. B.; Bose, S.; Fraser, J. D. & Bandyopadhyay, A. (2003). Micro-Machining Of PZT-Based MEMS, *American Ceramic Society Bulletin*, Vol.82, No.1, pp. 30–34

Newnham, R. E.; Skinner, D. P. & Cross, L. E. (1978). Connectivity and Piezoelectric-Pyroelectric Composites, *Material Research Bulletin*, 13, No.5 (1978) pp.525–536

Ohno, T.; Kunieda M.; Suzuki, H. & Hayashi, T. (2000). Low-Temperature Processing of ($PbZr_{0.53}Ti_{0.47}O_3$) Thin Films by Sol-Gel Method, *Japanese Journal of Applied Physics*, Vol. 39, No.9B, pp. 5429–5433

Pauer, L.A. (1973). Flexible piezoelectric materials, *IEEE International Convention Record*, Vol.21, pp.1–5

Pérez, J. (2004). Preparation and Characterization of Ferroelectric PZT Films for Electromechanical and Memory Applications", *Ph.D. Thesis Dissertation*, University of Aveiro, Portugal

Perez, J.; Vilarinho, P. M. & Kholkin A. L. (2004). High-Quality $PbZr_{0.52}Ti_{0.48}O_3$ Films Prepared by Modified Sol–Gel Route at Low Temperature, *Thin Solid Films*, Vol.449, No. 1-2, pp. 20–24

Pérez, J.; Vyshatko, N. P.; Vilarinho, P. M. & Kholkin, A. L. (2007). Electrical Properties of Lead Zirconate Titanate Thick Films Prepared by Hybrid Sol-Gel Method with Multiple Infiltration Steps, *Materials Chemistry and Physics*, Vol.101, No.2-3, pp.280–284

Polla, D. L. & Schiller, P. J. (1995). Integrated Ferroelectric Microelectromechanical Systems (MEMS), *Integrated Ferroelectrics*, Vol.7, No.3-4, pp. 359–370

Scheidegger, A. E. (1974), The Physics of Flow Through Porous Media, (3rd Ed.), ISBN 10-0802018491, University of Toronto Press, Toronto, Canada

Simon, L.; Le Dren, S.; & Gonnard, P. (2001). PZT and PT Screen-Printed Thick Films, *Journal of the European Ceramic Soc*iety, Vol.21, No.10-11, pp.1441–1538

Trolier-McKinstry, S. & Muralt, P. (2004). Thin Film Piezoelectrics for MEMS, *Journal of Electroceramics*, Vol.12, No.1-2, pp.7–17

TRS ceramic Data Sheet, "*Properties of TRS Soft Piezoceramics*", 8-3-98, (1998)

Tsurumi, T.; Ozawa, S.; Abe, G.; Ohashi, N.; Wada, S. & Yamane, M. (2000). Preparation of $PbZr_{0.53}Ti_{0.47}O_3$ Thick Films by an Interfacial Polymerization Method on Silicon

Substrates and Their Electric and Piezoelectric Properties, *Japanese Journal of Applied Physics*, Vol.39, No.9B. pp. 5604–5608

Tu, W. C. & Lange, F. F. (1995). Liquid Precursor Infiltration Processing of Powder Compacts 1. Kinetic Studies and Microstructure Development, *Journal of the American Ceramic Society,* Vol.78, No.12, pp. 3277–3282

Walter, V.; Delobelle, P.; Le Moal, P.; Joseph, E.; & Collet, M. (2002). A Piezo-Mechanical Characterization of PZT Thick Films Screen-Printed on Alumina Substrate, *Sensor and Actuators A-Physical*, Vol.96, No2-3, pp.157–166

Wang, Z.; Zhu, W.; Zhao, C. & Tan, O. K. (2003). Dense PZT Thick Films Derived from Sol-Gel Based Nanocomposite Process, *Material Science Engineering B*, Vol.99, No.1-3, pp.56–62

Wu, A.; Vilarinho, P. M.; Miranda Salvado, I. M.; Baptista, J. L.; de Jesus, C. M. & da Silva, M. F. (1999). Characterization of Seeded Sol-Gel Lead Zirconate Titanate Thin Films, *Journal of the European Ceramic Soc*iety, Vol.19, No.6-7, pp. 1403–1407

Xia, D.; Liu, M.; Zeng Y. & Li, C. (2001). Fabrication and Electrical Properties of Lead Zirconate Titanate Thick Films by the New Sol–Gel Method, *Material Science and Engineering B*, Vol. 87, No.2, pp. 160–163

Yang, C.; Liu, J.; Zhang, S. & Chen, Z. (2003). Characterization of $Pb(Zr,Ti)O_3$ Thin Film Prepared by Pulsed Laser Deposition, *Material Science Engineering B*, Vol.99, No.1-3, pp.356–359

Zhou, Q. F.; Chan, H. L. W. & Choy, C. L. (2000). PZT Ceramic-Ceramic 0-3 Nanocomposite Films for Ultrasonic Transducer Applications, *Thin Solid Films*, Vol. 375, No.1-2, pp. 95–99

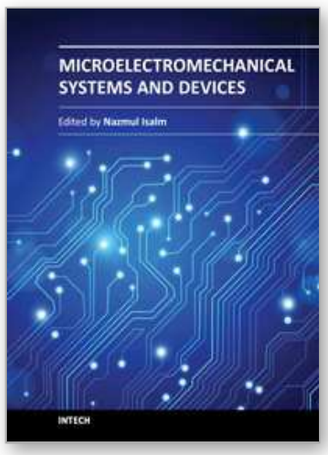

Microelectromechanical Systems and Devices

Edited by Dr Nazmul Islam

ISBN 978-953-51-0306-6
Hard cover, 480 pages
Publisher InTech
Published online 28, March, 2012
Published in print edition March, 2012

The advances of microelectromechanical systems (MEMS) and devices have been instrumental in the demonstration of new devices and applications, and even in the creation of new fields of research and development: bioMEMS, actuators, microfluidic devices, RF and optical MEMS. Experience indicates a need for MEMS book covering these materials as well as the most important process steps in bulk micro-machining and modeling. We are very pleased to present this book that contains 18 chapters, written by the experts in the field of MEMS. These chapters are groups into four broad sections of BioMEMS Devices, MEMS characterization and micromachining, RF and Optical MEMS, and MEMS based Actuators. The book starts with the emerging field of bioMEMS, including MEMS coil for retinal prostheses, DNA extraction by micro/bio-fluidics devices and acoustic biosensors. MEMS characterization, micromachining, macromodels, RF and Optical MEMS switches are discussed in next sections. The book concludes with the emphasis on MEMS based actuators.

INTECH
open science | open minds

InTech Europe
University Campus STeP Ri
Slavka Krautzeka 83/A
51000 Rijeka, Croatia
Phone: +385 (51) 770 447
Fax: +385 (51) 686 166
www.intechopen.com

InTech China
Unit 405, Office Block, Hotel Equatorial Shanghai
No.65, Yan An Road (West), Shanghai, 200040, China
中国上海市延安西路65号上海国际贵都大饭店办公楼405单元
Phone: +86-21-62489820
Fax: +86-21-62489821

IntechOpen